




Design, Formulation, *In-Vitro* and *Ex-Vivo* Evaluation of Atazanavir Loaded Cubosomal Gel

Ananda Kumar Chettupalli ¹, Madhubabu Ananthula ², Padmanabha Rao Amarachinta ², Vasudha Bakshi ², Vinod Kumar Yata ^{3,*}

¹ Department of Pharmaceutics, Centre for Nano-medicine, School of Pharmacy, Anurag University, Venkatapur, Ghatkesar, Medchal, Hyderabad, Telangana-500088, India

² Department of Pharmaceutics, Centre for Nano-medicine, School of Pharmacy, Anurag University, Venkatapur, Ghatkesar, Medchal, Hyderabad, Telangana-500088, India

³ Animal Biotechnology Centre, National Dairy Research Institute (NDRI), Karnal-132001, India

* Correspondence: vinodyata@gmail.com;

Scopus Author ID 36553530200

Received: 13.11.2020; Revised: 20.12.2020; Accepted: 21.12.2020; Published: 30.12.2020

Abstract: In this study, Atazanavir (ATZ) was designed into the Nano formulation called cubosomes to improve its bioavailability and curtail the adverse effects by the transdermal route delivery of ATZ - loaded cubosomes. Around twenty cubosomal formulations were formulated using a Central composite factorial design. The effect of glyceryl monooleate (GMO), surfactant (Pluronic F 127), and Cetyltrimethylammonium bromide (CTAB) were studied using processes of emulsification and homogenization. Different concentrations of independent variables on particle size distribution, zeta potential, and entrapment efficiency were determined. FTIR, DSC, X-ray, and SEM, TEM results established that the drug was encapsulated in the cubosomes. The results suggested that the optimal formula exhibited a particle size of 100 ± 7.9 - 345 ± 6.4 nm and entrapment efficiency ranging from 61 ± 4.6 - 93 ± 0.8 , zeta potential values ranging from -24.51 to -32.45 mV, polydispersity index values ranged from 0.35 ± 0.01 - 0.54 ± 0.02 of ATZ. The *in vitro* studies showed a controlled release pattern of drug release up to 24h. The ATZ cubosomal gel application on the *in vivo* absorption studies of the drug was studied in rats and compared with oral ATZ solution. The *in vivo* study results showed that the transdermal application of ATZ cubosomal gel considerably improves the absorption of drug compared to that of oral ATZ solution and found that the relative bioavailability is 4.6 times greater of oral ATZ solution. Thus it can be concluded that the ATZ cubosomal gel application via transdermal delivery route has the potential in increasing the bioavailability of the drug.

Keywords: ATZ-loaded cubosomes; central composite design; Pluronic F 127; bicontinuous structures; homogenization processes.

© 2020 by the authors. This article is an open-access article distributed under the terms and conditions of the Creative Commons Attribution (CC BY) license (<https://creativecommons.org/licenses/by/4.0/>).

1. Introduction

Antiretroviral (ARV) treatment guidelines currently recommend ARV regimens containing a Nucleos(t)ide Reverse Transcriptase Inhibitors (N(t)RTIs) based backbone with a Non-Nucleoside Reverse Transcriptase Inhibitor (NNRTI) or ritonavir-boosted Protease Inhibitor (PI/r). However, significant toxicity has been associated with N(t)RTI(s) and PI/r containing regimens. Recent data presented by Gupta *et al.* show that the combination of raltegravir (RAL) plus unboosted atazanavir (ATV) may be an alternative effective ARV regimen demonstrating good virologic and immunologic response [1]. Furthermore, the combination is well tolerated and has a low incidence of adverse effects [2]. Moreover, side

effects reported by Zhu *et al.* during a study in healthy subjects were generally “mild-to-moderate” in intensity. Common side effects were seen when both drugs were taken, such as jaundice and headache [3]. Ripamonti *et al.* evidenced that after five to seven months of therapy based on RAL plus ATV no patients discontinued treatment due to drugs used in therapy, adverse events. No one had grade 3 or 4 lab toxicity [4]. For these reasons, this combination of antiretroviral therapy based on RAL plus ATV attracts the scientific community's attention because both drugs have a good safety profile coupled with potent antiviral activity. Their combined use would avert nucleoside- and ritonavir-related toxicities.

Transdermal drug delivery is a non-invasive delivery of medications across the skin's surface through its layers to the circulatory system [5]. Because of its enormous advantages over conventional delivery systems, the transdermal drug delivery system remains of great interest for researchers [6]. This is because of its ability to deliver different drugs into blood, eliminate hepatic first-pass metabolism, and enhance patient compliance [7]. Cubosomes were selected as a nanocarrier because they possess many advantages. Cubosomes are formed by the fragmentation of lipid base in the presence of surfactant using excess water [8]. Cubosomes differ from emulsions. An emulsion is a biphasic system consisting of two immiscible liquids, one of which is finely and uniformly dispersed as globules throughout the second phase [9]. Cubosomes can penetrate skin and mucosa because of the similarity between their inner structure and epithelium cell; they can enhance drug bioavailability [10]. One more advantage of cubosomes is their hydrophilic, hydrophobic, and amphiphilic nature of drugs ranging from small molecules to large molecules.[11].

The lipophilic drug carrier has the ability to improve the therapeutic efficacy of the drug [12-14]. Cubosomes are nanostructured aqueous dispersions having a characteristic feature of dispersed particles. Their name, cubosomes, reflects their dispersion particle shape, consisting of cubic liquid crystalline phase consisting of highly twisted bi-continuous structures, two congruent non-intersecting water channels separated by continuous lipid bilayer [15-17].

Cubosomes can be prepared from biodegradable lipid materials like mono-glycerides such as monoolein (MO). MO forms bilayers of continuous inverted cubic phase separating two intercrossing water canals at NRT. Cubosomes are formed due to the emulsification of lipid phases in water [18-19]. These cubosomes are potential drug nanocarriers since they are tailored for solubilizing higher amounts of amphiphilic, hydrophobic, and hydrophilic drugs in their structures [20]. Moreover, cubosomes are greatly biocompatible and bio-adhesive nanoparticles. The presence of the same cubic phase structure between the cubosomes and stratum corneum has a penetration enhancing effect on the skin due to the stratum corneum's fluidization [21]. Furthermore, cubosomes are known to be skin-adhesive, flexible drug nanocarriers administered by transdermal as potential carriers in the drug delivery system.

Response surface methodology (RSM) is considered an efficient statistical technique used to reveal process parameters and their interactive effects [22-23]. The Central Composite design (CDD) is the main tool of response surface methodology design and has been successfully used to model and optimize the processes in many fields [24-26]. Atazanavir (ATZ) based cubosomes provide potential effects in the form of biocompatible and bio-adhesive transdermal dosage form with a decrease in ATZ side effects. Therefore, this study is aimed to prepare ATZ -loaded cubosomes and look for the parameters meters influencing the properties of MO-based cubosomes. Additionally, to assess the ability of cubosomes to act as a transdermal carrier in drug delivery.

2. Materials and Methods

Materials: Atazanavir (ATZ) were given by Hetero Labs, Hyderabad, as a source of glyceryl-monooleate (GMO), Pluronic® F-127 was purchased from Sigma-Aldrich Chemical Company. Ethanol was purchased from S.D. Fine chemicals, Mumbai. Cetyl-trimethyl-ammonium bromide (CTAB) was purchased from Loba Chemie, India. All other chemicals were of HPLC grade.

2.1. Experimental design.

An (Central composite design) experimental design with two factors, three levels (DESIGN EXPERT® software, version 12.0.12.0, Stat-Ease Inc. Minneapolis, MN, USA.) was adopted optimization of atazanavir cubosomes. The effect of three independent variables, namely GMO, Pluronic F127 and CTAB concentrations, and dependent variables are on cubosomal % Entrapment efficiency, % CDR, the particle size of ATZ-loaded cubosomes was evaluated. The analysis of the experimental data was performed by an ANOVA. The *Ex-vivo* and *in-vitro* drug permeation studies were performed with prior approval from the IAEC committee wide No. No.006/09/AGI/CPCSEA/2019/16.

Desirability was calculated for the selection of optimized formula, which was subjected to further evaluation. Table 1 shows the independent and dependent variables the actual and coded levels of variables used in the CCD. GMO (X1), F127(X2), and CTAB (X3) are defined as the independent variable. In contrast, entrapment efficiency (Y1), %Cumulative drug release (Y2), and Particle size (Y3) are defined as the dependent variable in this study. The experimental design included 20 experiments, and 5 center points are listed in Table 2. The dependent variable (Y) 's relevance to independent variables (X) is evaluated by a second-order polynomial equation. The model is described as follows:

$$Y = \beta_0 + \beta_1 X_1 + \beta_2 X_2 + \beta_3 X_3 + \beta_{12} X_1 X_2 + \beta_{13} X_1 X_3 + \beta_{23} X_2 X_3 + \beta_{11} X_1^2 + \beta_{22} X_2^2 + \beta_{33} X_3^2$$

Where Y is the response; X1, X2, and X3 are the independent Factors; β_0 is the intercept coefficient; β_1 , β_2 , and β_3 are the linear interaction coefficients; β_{13} , β_{12} , and β_{23} are the squared effects terms and β_{11} , β_{22} , and β_{33} are the interaction coefficients. The ANOVA analysis of data obtained from the experiments is carried out by Design-Expert software (trial version 12.0.12.0, Stat-Ease, USA).

Table 1. Levels of three independent variables used in Central composite design.

Independent variable	Coded symbol	Levels		
		-1	0	+1
GMO (Glyceryl monooleate) (mg)	X1	100	175	250
Pluronic F127(mg)	X2	10	25	40
CTAB (Cetyltrimethylammonium bromide) (mg)	X3	3	6.5	10
Dependent Variables	Coded symbol	Levels		
Entrapment Efficiency (%)	Y1	Maximize		
Cumulative Drug Release (%)	Y2	Maximize		
Vesicle Size (nm)	Y3	Minimum		

2.2. Preparation of ATZ-loaded cubosomal dispersions.

ATZ-loaded cubosomal formulations were designed and developed as per the Nasr method [22]. Atazanavir was weighed into a glass vial and heated at 40°C until free-flowing. Aqueous solutions containing different GMO concentrations, Pluronic F-127, and CTAB were dissolved in the obtained molten mixture by continuous stirring. Deionized water (0.5 mL) was added to the mixture drop-wise while maintaining a high, stirring speed at room temperature

to achieve a homogenous state (KLM-307, Elektrocraft Ind.pvt.LTD) at 40°C, amplitude 80%, pulse cycle 1 for 30 min until a milky dispersion was formed. The mixture was equilibrated for 48 h at room temperature. To prepare the Cubosomal dispersion, the obtained gel was dispersed with the distilled water by vortex at high speed for 3 min. Then the cubosomal dispersions were sonicated for 15 min using water bath sonicator (CD-4820, Citizen India). Twenty formulae of different combinations were prepared, as shown in Table 2.

2.3. Determination of particle size, polydispersity index (PDI).

The mean particle size, PDI of ATZ-cubosomes were determined using Zetasizer Nano-ZS (Malvern Instrument Ltd., Worcestershire, UK) at 25°C, based on photon correlation spectroscopy and electrophoretic mobility principles. All samples were appropriately diluted with deionized water before measurements were taken. The cubosomes formulations' zeta potential were determined using a zeta sizer (Malvern instrument, UK). They were diluted in the ratio of 1:2500 (v/v) with distilled water.

2.4. Entrapment efficiency.

In order to determine entrapment efficiency (EE %), the total amount of ATZ incorporated in 1 mL cubosomal dispersion was determined after the addition of 9.0 mL ethanol. The resultant solution was assayed for the total ATZ content by UV spectrophotometer (Lab India UV-320, Mumbai, India) at 249 nm using ethanol as blank. High-Speed centrifugation was used to separate free ATZ from cubosomal dispersion [27]. One mL of freshly prepared ATZ-loaded cubosomal dispersions was diluted to 10 mL with purified water, and 3 mL of the diluted samples were placed in Amicon Ultra 3000 MWCO centrifuge tubes (Millipore, USA) and centrifugation at 9000 rpm for 45 min at 4°C. Free ATZ contained in the filtrate was measured spectrophotometrically at 249 nm [28]. The amount of entrapped ATZ was calculated by subtracting the determined amount of ATZ in the filtrate from the total amount of drug incorporated in 1 mL cubosomal dispersion. The entrapment efficiency (EE %) was calculated using the equation:

$$EP = [(C_t - C_r) / C_t] * 100$$

Where,

C_t, concentration of total Atazanavir,

C_r, concentration of free Atazanavir.

2.5. Optimization and validation.

To attain an optimum cubosomal formulation that fulfills the previously decided constraints on the % entrapment efficiency, % CDR, Particle size, Zeta potential, PDI (Table 2), simultaneous optimization technique via the desirability function was applied using Design® expert software. The suggested optimized formulation was prepared, and the required dependent variables were evaluated as previously. To objectively assess the validity of the final selected models, the 95% two-sided prediction intervals (95% PIs) for the predicted values were calculated. The mean of the measured values (actual value) for each dependent variable of the optimized formulation was checked to ascertain if it lied within the 95% PIs or not [29]. Additionally, the actual values were also compared to the predicted values using % prediction error.

$$\% \text{ prediction error} = 100 [Y_m \text{ predicted} - Y_m \text{ actual}] / Y_m \text{ predicted} \quad (2).$$

2.6. Preparation of gel containing ATZ-loaded cubosomes.

The gel formulation containing ATZ-loaded cubosomes was prepared. Briefly, cubosomal dispersion of optimized formulation was mixed with carbopol 934 1% and left to soak overnight. A mixture of absolute ethanol, glycerin, and deionized water was added portion-wise with continuous stirring until the homogeneous gel is obtained. The final carbopol 934 and ATZ concentrations were 3% and 0.01% w/w, respectively, concerning the gel's final weight.

Table 2. CCD Experimental design and response for the dependent variables.

Std	Run	GMO (mg)	Pluronic F 127 (mg)	CTAB (mg)	%EE	%CDR	Particle size (nm)	PDI	Zeta potential (mV)	Desirability
9	1	48.8655	25	6.5	82±1.1	84±4.6	300±4.6	0.54±0.01	-26.81	0.791
14	2	175	25	12.3863	72±2.6	68±6.1	275±8.6	0.52±0.02	-32.45	0.681
3	3	100	40	3	89±2.4	70±5.8	150±7.6	0.48±0.03	-29.43	0.846
15	4	175	25	6.5	93±0.9	90±1.3	168±5.6	0.35±0.01	-24.51	0.879
19	5	175	25	6.5	93±0.8	90±1.1	140±6.4	0.32±0.03	-24.53	0.978
2	6	250	10	3	66±3.4	92±1.2	310±8.4	0.43±0.01	-31.56	0.843
13	7	175	25	0.613725	69±4.6	78±2.6	264±8.2	0.42±0.01	-30.60	0.681
6	8	250	10	10	88±1.7	75±5.7	100±9.1	0.39±0.02	-24.91	0.789
7	9	100	40	10	65±3.6	70±4.9	345±6.4	0.42±0.02	-28.73	0.761
12	10	175	50.2269	6.5	73±1.4	65±6.4	160±5.8	0.41±0.01	-27.62	0.879
18	11	175	25	6.5	93±0.7	90±1.2	150±3.7	0.40±0.03	-25.40	0.941
1	12	100	10	3	67±3.6	70±5.6	430±7.9	0.58±0.02	-26.13	0.861
16	13	175	25	6.5	93±1.2	90±1.0	155±6.4	0.38±0.02	-24.50	0.923
10	14	301.134	25	6.5	79±2.7	80±3.5	100±7.9	0.39±0.01	-28.32	0.845
5	15	100	10	10	86±2.2	87±1.6	230±6.4	0.49±0.03	-28.11	0.645
4	16	250	40	3	72±2.9	85±2.3	120±9.2	0.51±0.02	-29.72	0.789
20	17	175	25	6.5	93±1.2	92±1.1	150±8.7	0.35±0.02	-24.53	0.856
8	18	250	40	10	61±4.6	60±5.4	253±5.6	0.43±0.02	-29.41	0.843
17	19	175	25	6.5	93±0.7	90±0.6	150±4.5	0.45±0.02	-24.50	0.910
11	20	175	-0.226892	6.5	78±1.3	80±2.3	215±8.8	0.48±0.01	-32.41	0.875

2.6.1. Evaluation of gel formulation.

2.6.1.1. pH evaluation.

The pH of the gel was determined using a pH meter (SAB 5000 Lab India), which was calibrated before every use with standard buffered solutions of pH 4, 7, and 10.

2.6.1.2. Viscosity measurement.

Gel viscosity was determined using the Brookfield viscometer (Brookfield Viscometer, LVDV-11+Pro) using spindle S06 at a rotation speed of 60 rpm. The gel's measurement samples were allowed to settle over 30 min at room temperature before the measurements were taken.

2.6.1.3. Effect of storage.

The effect of storage on the optimized ATZ-loaded cubosomal gel formulation was implemented by placing freshly prepared samples of the gel at room temperature (25 °C ± 2 °C) for 3 months. The cubosomal gel was then evaluated for its pH, percent drug content, and viscosity at different storage stages.

2.7. Physicochemical characterization of optimum cubosomal dispersion.

The cubosomal formula that fulfilled the implemented Central composite design's optimum criteria was subjected to further investigation and characterization.

2.7.1. Fourier transform infrared (FTIR).

An appropriate amount of KBr was dried under an infrared lamp, mixed with the different samples (i.e., pure ATZ, Pluronic F 127, alcohol, Poloxamer 407). Finally, cubosomal powder was identified using an FTIR spectrometer (Bruker, Alpha). It was made into a plate at a pressure of 300 kg/cm². The plate was scanned by an infrared spectrometer at 400–4000 wave-number with a resolution of 2 cm⁻¹ [30].

2.7.2. Differential scanning calorimetry (DSC).

DSC was performed using a thermal analysis system (DSC- 60, Shimadzu, Japan) to identify possible changes in the physical state of ATZ entrapped in cubosomal dispersion. DSC was performed on pure ATZ powder, GMO, Pluronic F 127, CTAB, Ethanol, cubosomal dispersion, and cubosomal gel. The cubosomal samples of about 5 mg were subjected to heating at a rate of 10 °C/min in an aluminum pan under a nitrogen atmosphere condition. A similar empty pan was used as the reference [30].

2.7.3. X-ray diffraction (XRD).

X-ray diffraction patterns of the prepared cubosomal dispersion as well as pure ATZ, Cubosomal dispersion, and cubosomal gel samples were obtained using the X-ray diffractometer (PHILIPS® X'pert multi-purpose diffractometer) with Cu as tube anode. The diffractograms were recorded under the following conditions: the voltage 40 kV, the current 30 mA, the steps 0.02°, and the counting rate 1 s/step at room temperature. Data were collected using a scattering angle (2θ) ranged 4–60°.

2.8. Surface morphology using SEM& TEM.

The study of cubosomal dispersion and cubosomal gel surface morphology was studied by using scanning electron microscopy. The sample of formulations has first adhered to the carbon-coated metallic stub. This was sputter-coated with a Platinum coating machine (JFC-1600 Auto fine coater, JEOL, Tokyo, Japan) and mounted in SEM (JSM-6510LA, JEOL, Tokyo, Japan) for surface analysis. Imaging was carried out in a high vacuum [23-25].

To determine the morphology of cubosomal dispersion, a transmission electron microscope (JEOL, Japan), model JEM-2100 equipped with super twin lens, was used. A droplet of cubosomes dispersion was placed on a carbon-coated copper grid and then stained with 1% sodium phosphotungstate solution; after that, the excess fluid was removed by an absorbent filter paper, and finally, the sample was subjected to dry for 15 min at room temperature for studying the morphology of cubosomes.

2.9. In vitro drug release study.

In-vitro release studies were performed by unjacketed vertical Franz diffusion cells with a diffusional surface area of 5.96 cm² and 20 mL of receptor cell volume. Before initiation of the study, the dialysis membrane was immersed in a buffered solution (pH 7.4). Formulation equivalent to 5mg of Atazanavir was placed in the donor compartment. The receptor

compartment consisting of PB pH 7.4 (containing 0.02% w/v of ethanol to retard microbial growth) was maintained at $37 \pm 2^\circ\text{C}$ under constant stirring up-to 24 hrs. The donor chamber and the sampling port were covered with a lid to prevent evaporation during the study. Aliquots of 5 mL were withdrawn periodically at different time intervals (0, 5, 10, 15, 30, 1, 2, 3, 4, 5, 6, 7, 8, 12, and 24hrs) replaced with equal volume to maintain constant receptor phase volume. At the end of the study, the samples were suitably diluted, and the amount of the drug was determined spectrophotometrically [31-33].

2.10. *Ex vivo* skin permeation study.

A freshly excised hairless abdominal rat skin was selected and placed between the compartments of donor and receptor of Franz-type diffusion cells with an effective permeation area of 2 cm^2 and with the stratum corneum facing the donor compartment. The receptor solution consisted of 200 mL of phosphate buffer pH 7.4 maintained at $37 \pm 0.5^\circ\text{C}$ and continuously stirred with a magnetic bar at 60 rpm. Then, 1 mL of the cubosomal dispersions and ATZ aqueous solution was added to the donor compartment. Samples from the receptor compartment (1 mL) were withdrawn periodically over 24 h and analyzed for drug content spectrophotometrically at 249 nm. The 1 mL aliquots were substituted by an equal volume of phosphate buffer pH 7.4 maintained at $37 \pm 0.5^\circ\text{C}$. At the end of the experiment and in order to determine the amount of ATZ deposited in the skin, the rat skin was cleaned 5 times with a cotton cloth soaked in ethanol. The skin was then finely divided and immersed for 6 h in 6 mL of ethanol under constant stirring at room temperature. Extraction dispersions were centrifuged at 4000 rpm for 15 min and filtered through a $0.22\text{ }\mu\text{m}$ filter. Diffusion cells free of formula were also established. Samples collected from permeation of drug-free systems were used as a blank, and filtrates were studied at 249nm using a spectrophotometer. The slope of the curve plotted for the cumulative amount of ATZ infused per unit area as a function of time was used to determine the drug steady-state flux (J_{ss}) [34-36]. The permeability coefficient (k_p) of ATZ through the skin from the investigated cubosomes was calculated as follows:

$$K_p = J_{ss}/C$$

Where J_{ss} : steady-state drug flux

C: drug concentration in the donor compartment.

2.11. *Statistical analysis.*

Statistical analysis (SPSS program version 17 software) was of the *in-vitro* studies were performed using one-way analysis of variance (ANOVA), followed by the least significant difference (LSD) as a post hoc test., was applied using. The mean differences between the samples were considered significant if $P < 0.05$.

3. Results and Discussion

3.1. *Preparation of ATZ-loaded cubosomes nanoparticles.*

The ATZ cubosomal dispersion was prepared devoid of organic solvents, making a way to green synthesis in drug delivery systems based on lipid carriers. Ethanol aqueous solution was used as a steric barrier due to its absorption to the surface as an emulsion droplet, preventing emulsion droplets' aggregation and stabilizing. Ethanol forms small particles with uniform distribution, which can be easily dispersed in an aqueous medium. Stabilizers were

used in cubosomal dispersion for modifying the surface properties and stability. The stabilization of ATZ cubosomal dispersion by Pluronic F 127 formed due to the adsorption of GMO, CTAB moieties into the outer surface of the cubosomal dispersion, which intern resulted in the inverted-type self-assembled lipid nanostructure from the surrounding aqueous medium, whereas the GMO copolymer's hydrophilic moieties dangled in the water. Increasing the concentration of Pluronic F 127 in the cubosomes formulations allowed smaller droplets to form by increasing the interfacial stability of cubosomal nanoparticles.

3.2. Determination of particles size, PDI and zeta potential.

The particle size analysis for cubosomal dispersion loaded with ATZ exhibited particle size values within the nano range (100 ± 7.9 – 345 ± 6.4 nm). As indicated in Table 1, the particle size of cubosomes is indirectly proportional to the increase in Pluronic F 127 concentration. Upon reducing Pluronic F 127 concentration, larger size cubosomes nanoparticles were formed due to the condensed interfacial stability and an insufficient amount of the surfactant, leading to aggregation of nanoparticles. The particle size distribution of the cubosomes nanoparticles specified by the polydispersity index values ranged from 0.32 ± 0.03 to 0.58 ± 0.02 , which was an acceptable range. The higher values of zeta potential deliver sufficient electric repulsion, which in turn prevents particle aggregation. The results of the potential zeta study show that ATZ-loaded cubosomes nanoparticles carried a negative charge with mean values of -24.51 to -32.45 . This might be due to the presence of the GMO, Pluronic F 127. Moreover, the negative surface charge may be due to the CTAB hydroxyl group. In general, Pluronic F 127 adding to the cubosomal dispersion medium resulted in negative charge values of cubosomes due to the interaction between Pluronic F 127 hydroxyl ions with the aqueous medium. Particle charge is an important parameter suggested by Kohli and Alpar as the only negatively charged particles are able to infuse through the skin due to the channels formed by the repulsive forces between negatively charged skin lipids and particles.

3.3. Cubosomes nanoparticles encapsulation efficiency (EE %).

The formulated cubosomes nanoparticles were mainly composed of the lipophilic material GMO and both Pluronic F 127 and CTAB surrounding the nanoparticles. It is estimated that cubosomes nanoparticles can carry and deliver lipophilic drugs that can dissolve in lipid nanostructure. Different formulations were compared to assess the amount of drug incorporated in the nanoparticles. It was found that due to the strong affinity between ATZ and the GMO in the cubosomes nanoparticles, it was 'grabbed' in the liquid crystal structure. Thus the encapsulation efficiency values were ranged from 61 ± 4.6 to $93 \pm 0.8\%$. Such high drug encapsulation efficiency is desirable to produce a therapeutic effect with less volume.

3.4. Selection of the optimum formula.

The analysis of formulations' variables showed that there is a strong relationship between GMO/Pluronic F 127 ratio and CTAB concentration and EE %, particle size distribution, and %CDR. Three-dimensional response surface diagrams were plotted to emphasize the effects of the interaction of the Pluronic F 127, CTAB, and GMO concentrations on particle size, EE %, and % CDR, respectively.

The independent variables and their interactions on dependent responses were studied using RSM and represented graphically by 3D surface plots. The effect of the amount of GMO,

amount of Pluronic F127, and amount of CTAB on % EE, % CDR and vesicle size, are represented in Figure 1. When % EE (Y1) was indicated as the response, a good correlation was shown between observed and predicted values as revealed by R^2 of 0.9092 (Table 3 and 4). Thus Y1 was significantly influenced by amounts of A, B, C and their interactive term (ABC) and polynomial model of lipid concentration A^2 with a $p < 0.0001$. The magnitude of the positive coefficient (328.21) of the term suggests that elevated levels of GMO, Pluronic F127, and CTAB concentrations in the formulation could increase the %EE drastically. The size of Cubosomes depends on GMO concentration can be explained in terms of the tendency of GMO to coalesce at high GMO concentration. Increasing GMO content in the cubosomal formulation leading to higher surface tension and thus increased the %EE. Figure 1(A) and (B) show the response surface model for %EE in response to the investigated factors. The independent variables have a positive influence on %EE. Figure 1(C) and (D) showed a linear relationship between the amount of GMO and %CDR of Cubosomal dispersion. Quantitative estimation of the significant models indicated that Pluronic F127 concentration had the prime influence on the % CDR for its large positive coefficient (+7.59), suggesting that increasing the amount of Pluronic F127 increased the CDR and the amount of CTAB has little effect on the % CDR in the formulation (Equation (1-3)). A high concentration of Pluronic F127 results in increasing the %CDR. Enhanced drug release may be due to micelles' formation at increased Pluronic F127 concentration, resulting in sufficient spare space to accommodate more drugs. This tendency could be attributed to the high lipophilicity and limited water solubility of ATZ. From Figure 1(E) and (F), the effect of formulation type and process variables on Particle size can be evaluated. When the amounts of GMO and Pluronic F127 were altered from lower to higher levels, significant vesicle size changes were noticed, but at low levels of Pluronic F127 amount alone, an increasing marginal trend in vesicle size was observed. This result implied that Pluronic F127 concentration showed a promising effect on the vesicle size, confirmed by a statistical ANOVA result. Point desirability suggested by Design-Expert® software actual and predicted values for entrapment efficiency and percent cumulative drug release and particle size (Figure 2).

Table 3. Analysis of variance in RSM and regression analysis predicted a second-order polynomial model for entrapment efficiency.

	Y1 (% EE)			Y2 (Cumulative % DR)			Y3 (Vesicle size)		
Model	R^2	Adjusted R^2	Predicted R^2	R^2	Adjusted R^2	Predicted R^2	R^2	Adjusted R^2	Predicted R^2
Linear	0.0489	0.1294	0.4837	0.2132	0.0657	0.2207	0.2836	0.1493	0.2425
2FI	0.3985	0.1209	0.5600	0.4662	0.2198	0.2586	0.7463	0.6292	0.2228
Quadratic	0.9882	0.9775	0.9092	0.9729	0.9485	0.8130	0.9780	0.9583	0.8470
<i>p</i> value	≤ 0.0001			≤ 0.0001			≤ 0.0001		

Table 4. ANOVA analysis of dependent parameters.

Parameter	Data Source	Degree of Freedom	Sum of squares	Mean of squares	F Value	<i>p</i> -Value
% EE	Model	9	2302.44	255.83	92.84	<0.0001
	Residual	10	27.56	2.76		
	Lack of fit	5	24.72	4.94		0.0164
	Pure error	5	2.83	0.5667		
% Cumulative DR	Model	9	1985.62	220.62	39.87	<0.0001
	Residual	10	55.33	5.53		
	Lack of fit	5	9.30	5.26		0.0462
	Pure error	5	1.77			
Vesicle size	Model	9	1496.05	16623.04	49.47	<0.0001
	Residual	10	3360.40	336.04		
	Lack of fit	5	2939.57	587.91	6.99	0.0262
	Pure error	5	420.83	84.17		

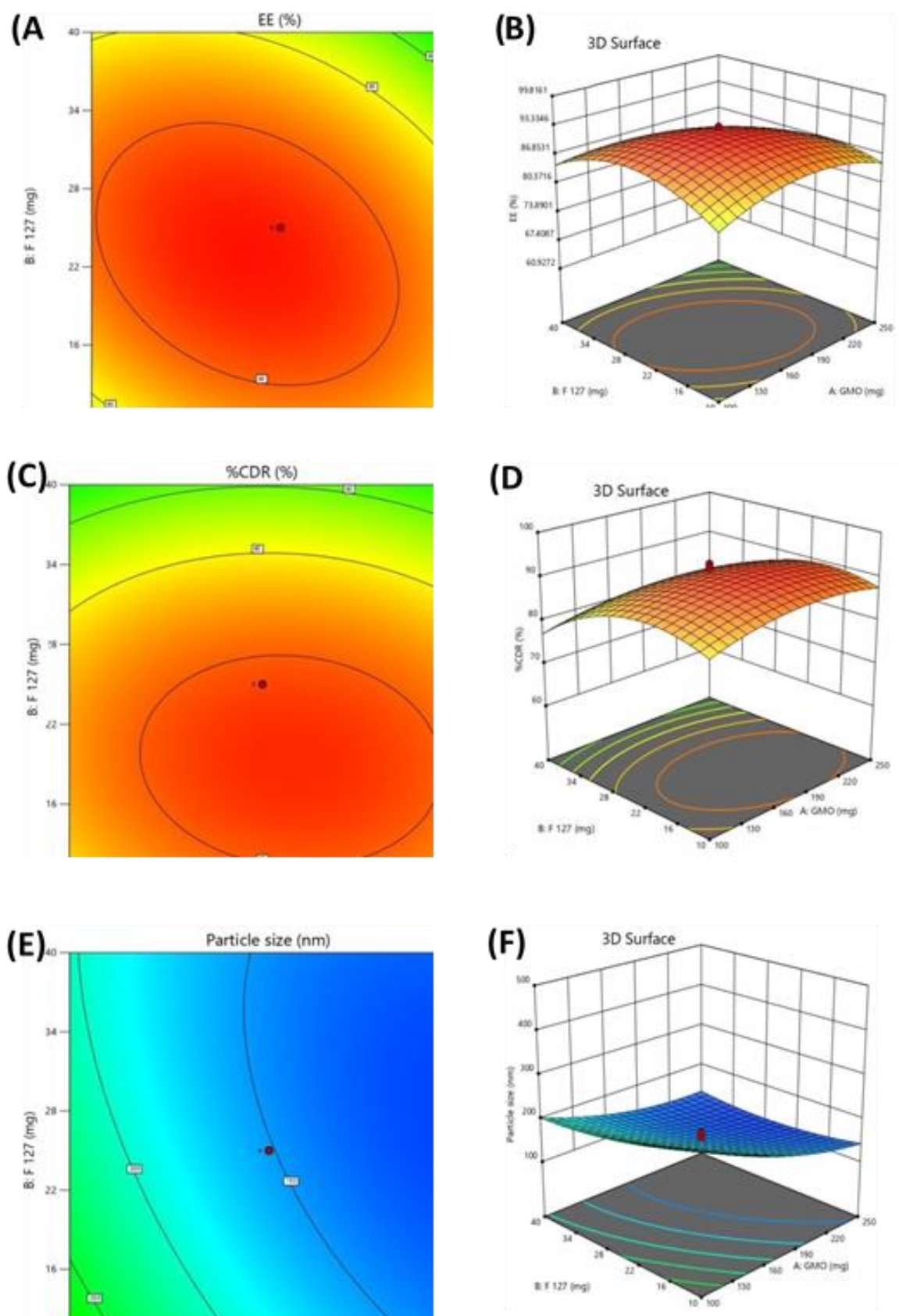


Figure 1. Contour plots and response surface plots showing the interactive effects Point desirability as suggested by Design-Expert® software Effect of the interaction of the Pluronic F 127, GMO and CTAB concentrations on A & B entrapment efficiency %, C & D %CDR and E & F particle size distribution.

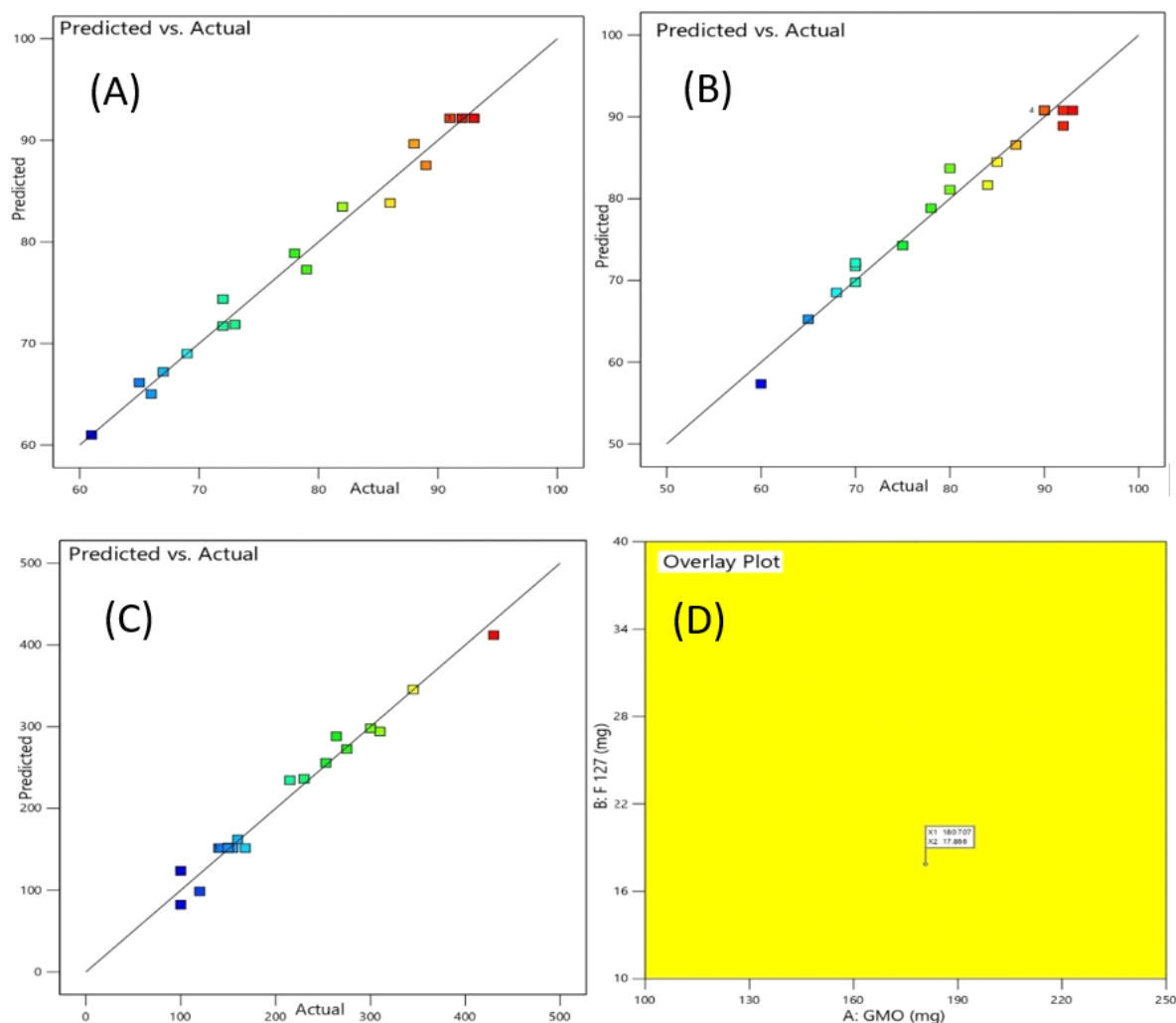


Figure 2. Point predictions (color points by the value of A. entrapment efficiency, B. % CDR, C. particle size and D. total overly plot of design) as suggested by Design-Expert® software actual and predicted values

3.5. Fourier transform infrared (FT-IR) studies.

FTIR spectra of ATZ (Pure API), GMO, Pluronic F127, ethanol, cubosomal dispersion, and cubosomal gel are shown in Figure 3.

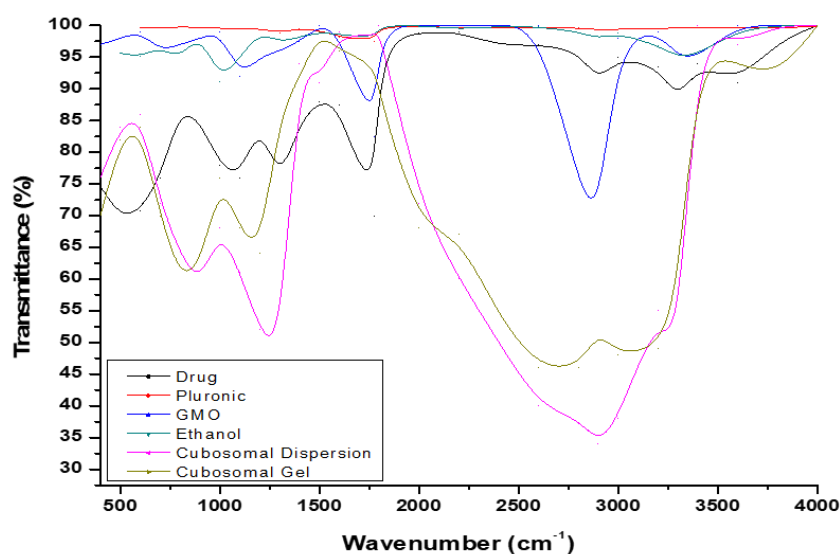


Figure 3. FTIR Spectral Studies.

3.6. DSC.

DSC was carried out to determine the crystalline properties of the loaded ATZ in cubosomal nanoparticles (F5) compared with pure ATZ, CTAB, Pluronic F 127, and GMO. The DSC thermogram of pure ATZ showed a characteristic peak at 163.48°C, corresponding to its melting point Figure 4.

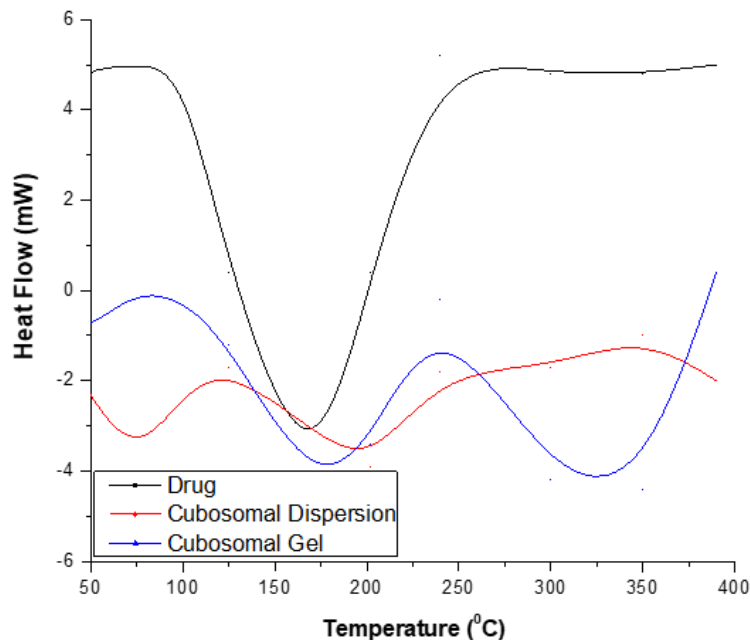


Figure 4. DSC thermogram of A. ATZ, B. GMO, C. Pluronic F127, D. CTAB, E. cubosomal dispersion and G. cubosomal gel.

3.7. X-ray diffraction studies.

In order to further confirm the physical state of ATZ, X-ray diffraction patterns of the prepared ATZ-loaded cubosomes, as well as the pure drug powder samples, were obtained (Figure 5). The diffractogram of the pure ATZ clearly showed strong characteristic peaks within the range of 2θ 10–30°; meanwhile, those characteristic peaks disappeared in ATZ loaded cubosomal nanoparticles (F5), indicating that the drug is either molecularly dispersed in cubosomes or possibly transformed into an amorphous form.

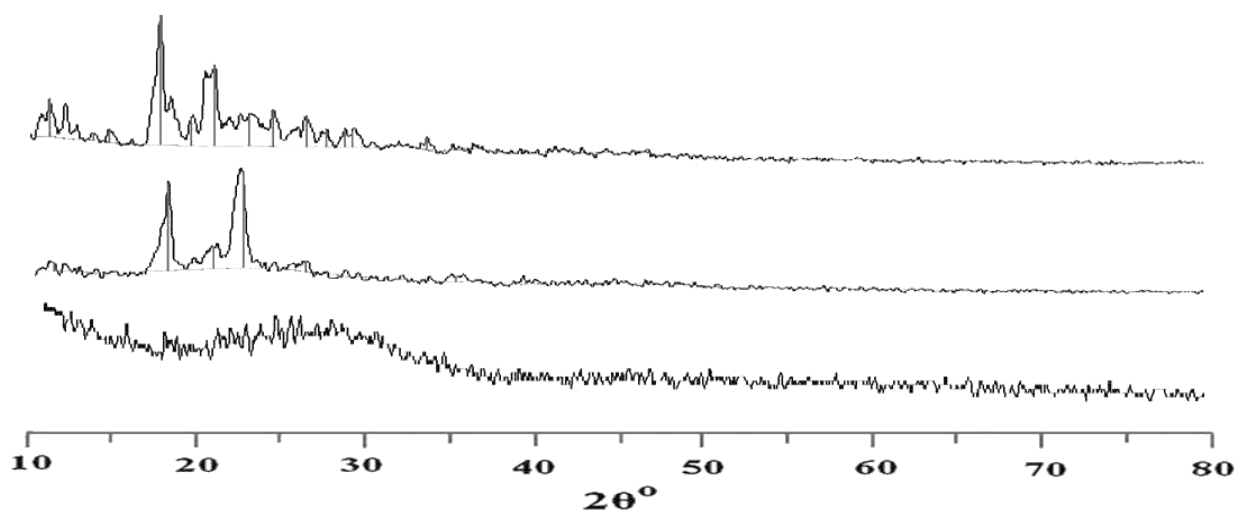


Figure 5. XRD diffractograms of A. Pure ATZ, B. cubosomal dispersion, and C. cubosomal gel.

3.8. Cubosomes nanoparticles morphology.

The cubosomal dispersion was studied for surface morphology at 30.0 kV magnification using SEM. The morphology of nanoparticles was found to be nearly spherical in shape, exhibited polydispersity, and possessed a smooth surface shown in Figures 6A and B.

Figure 6 C and D shows TEM images taken for optimized cubosomal dispersion (F5) and Cubosomal gel formulations. Cubic shapes of particles with zero mean curvature. However, a small population of hexagonal vesicles was observed. Particle sizes were in the nano-range and were well disconnected from each other. Cubosomes nanoparticles F5 showed smaller particles size. These findings are verified before by particle size and can be elucidated by the presence of a larger amount of Pluronic F 127 adsorbed on the cubosomes surface, which acts as a coating layer for stabilizing the surface area of nanoparticles.

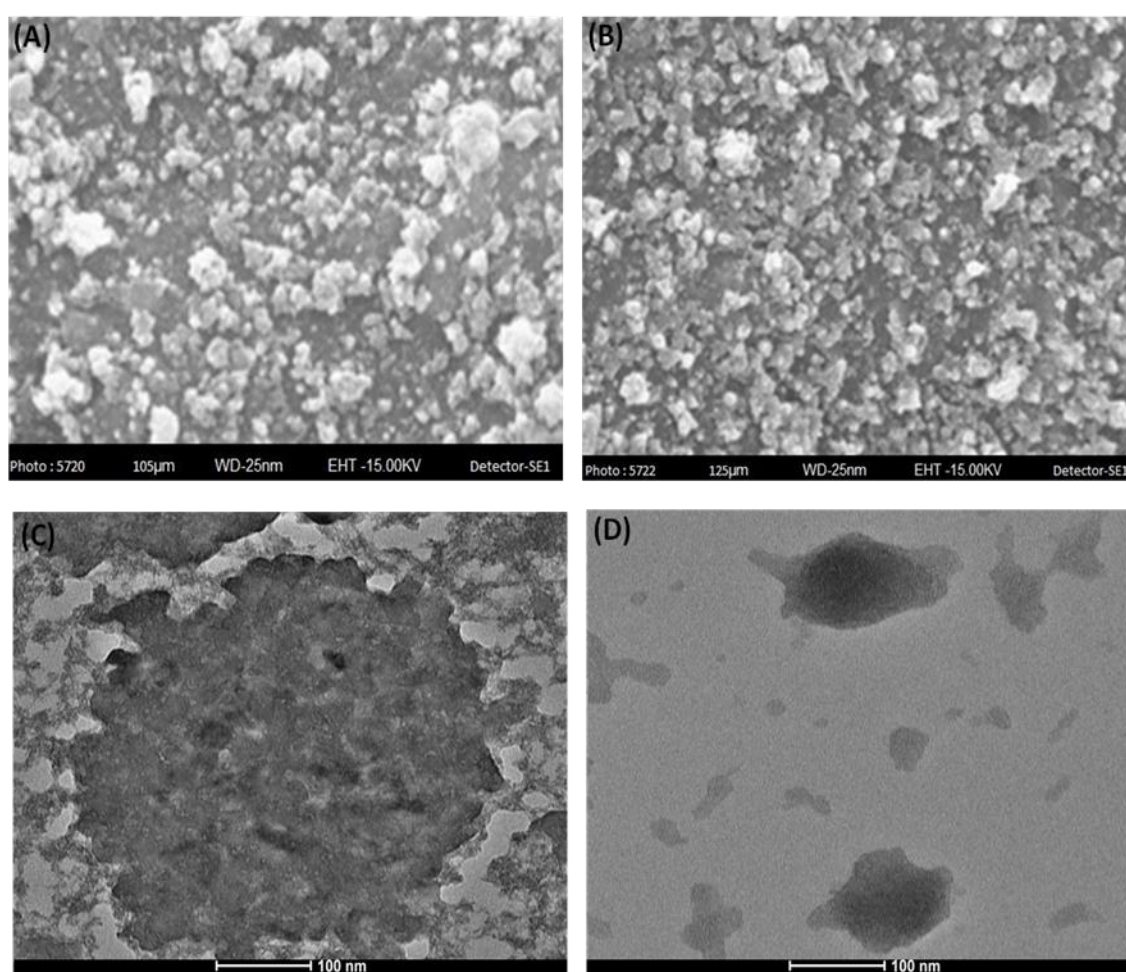


Figure 6. SEM micrograph of A. cubosomal dispersion b. cubosomal gel& TEM micrograph of C& D. cubosomal dispersion cubosomal gel.

3.9. Ex vivo permeation study.

Animal skin models have been successfully utilized as alternatives for human skin. Accordingly, the rat skin is considered a successful *ex vivo* model for studying the different drug carrier permeation systems. Figure 7 showed the cumulative amount of ATZ permeated through a unit area of abdominal rat skin from formulae F5 and cubosomal gel compared with aqueous ATZ solution. The calculated permeation parameters are illustrated. Evidently, no lag phase was identified. ATZ was detected in the receptor compartment after the first hour,

indicating the rapid drug release and its permeation across the skin. Similar results were previously reported in the literature.

All tested preparations showed relatively low amounts of ATZ released within the first 1.5 h, but the amount of ATZ released was significantly ($P < 0.05$) higher for F2 ($1409.29 \pm 150 \mu\text{g}/\text{cm}^2$) after 24 h compared with those of cubosomal dispersion ($1100 \pm 68.17 \mu\text{g}/\text{cm}^2$) and ATZ aqueous solution ($890.45 \pm 324.61 \mu\text{g}/\text{cm}^2$). It was obvious that the amount of ATZ deposited in the skin of F5 and cubosomal dispersion was 1.54 and 1.06 times greater than that of ATZ aqueous solution, respectively. This is favored when ATZ deposition in the skin is needed in certain dermatological conditions such as atopic dermatitis, actinic keratosis, and psoriasis.

The amount of ATZ deposited in the skin of cubosomal dispersion is relatively lower than that of F5. This may be attributed to the high zeta potential value of F5 because of the higher amount of CTAB used in F5 than that in remaining formulations. It was previously reported that the positively charged nano-emulsions containing phytosphingosine were found to be more effective in terms of skin diffusion of fludrocortisone acetate and flumethasone pivalate through porcine skin than the negatively charged ones. The permeation parameters are illustrated. The transdermal flux (J_{ss}) was determined from the slope of a Cartesian plot of the collective amount of drug present in receptor compartment versus time; meanwhile, ER2 enhancement ratio is the ratio of the amount of drug deposited from formulation to drug solution. ER3 enhancement ratio is the ratio of transdermal flux from formulation to drug solution. The steady-state drug flux (J_{ss}) values for ATZ aqueous solution, cubosomal dispersion, and F5, were nearly 28.64 ± 5.1 , 42.37 ± 2.1 , and $56.51 \pm 4.3 \mu\text{g}/\text{cm}^2 \cdot \text{hr}$, respectively; meanwhile, the permeability coefficient (k_p) values for ATZ aqueous solution, cubosomal dispersion, and F5, were 0.005 ± 0.002 , 0.009 ± 0.001 , and $0.013 \pm 0.002 \text{ cm}/\text{h}$. The high values of J_{ss} and k_p for F5 could be due to the higher amounts of GMO and Pluronic F127 in F5 compared with cubosomal dispersion and ATZ solution as it was previously reported that both GMO and Pluronic F127 are penetration enhancers.

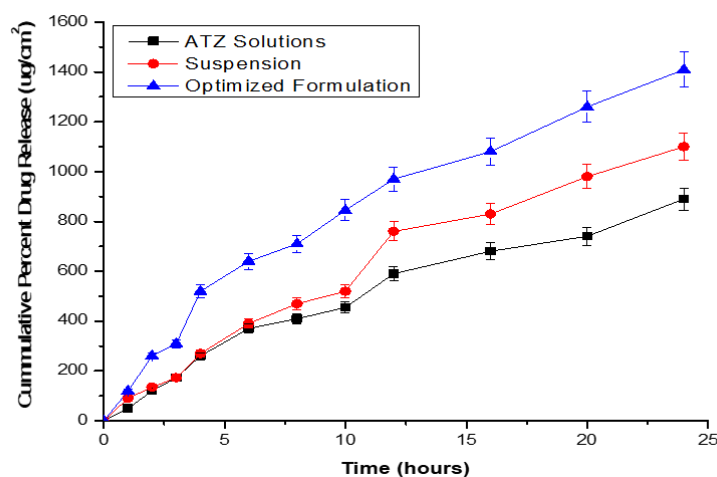


Figure 7. *Ex vivo* permeation studies of ATZ-loaded cubosomal Suspension F5, Cubosomal Gel compared with ATZ aqueous solution through excised rat skin.

3.9.1. Characterization of cubosomal ATZ gel.

The ATZ cubosomal gel drug content was estimated by dissolving 1 gram of gel in 8 mL ethyl alcohol. The volume was made up to 10 mL. Later 1 mL of solution was diluted with ethyl alcohol and measured spectrophotometrically at λ_{max} 249 nm. The drug content was

99.18 ± 0.63% (Figure 8), and the measured pH of the gel was 6.02 ± 0.05, which lies within the acceptable pH range of the skin. The cubosomal ATZ gel viscosity was 14,635 ± 296 (cP), which complies with the optimum gel viscosity range 13,000–16,000 (cP) Table 5.

3.9.2. Effect of storage.

After 3 months of storage of the freshly prepared ATZ-loaded cubosomal gel formulation at room temperature (25 °C ± 2 °C), the drug content, pH, and gel viscosity were 99.61 ± 0.28%, 5.95 ± 0.03, and 14,620 ± 125 cP, respectively. These results were found to be statistically insignificant ($P > 0.05$, paired t-test) compared with the same results obtained before storage, indicating the stability of ATZ-loaded cubosomal gel when stored at 25 °C ± 2 °C.

3.10. In vivo absorption study.

The parameters of LC-MS/MS method were validated according to ICH guidelines. The method showed high accuracy and precision with linear regression in the range of analysis. The mean (±SD, n = 6) plasma ATZ concentration-time profiles following administration of single doses (0.03 mg/kg) of oral ATZ solution and topical ATZ-loaded cubosomal gel to fasted rats were shown in Figure 7. It was obvious from ATZ plasma concentration-time profile that ATZ shows two absorption peaks for both oral solution and transdermal cubosomal gel. The second absorption peak is attributed to entero-hepatic circulation. This finding is in good agreement with previously reported results. The bioavailability parameters (C_{max} , T_{max} , and AUC_{0–48}) were calculated from the individual ATZ plasma concentration-time curves. The mean values ± SD are presented.

The obtained C_{max} after oral administration was 0.31 ± 0.17 ng/mL at T_{max} 3.15 ± 1.82 h, which indicated that ATZ is rapidly absorbed when given orally. However, a significantly higher value of C_{max} (0.86 ± 0.23 ng/mL at 13.80 ± 4.60 h) was observed after transdermal application of ATZ cubosomal gel (Table 6). The significantly delayed higher C_{max} values of ATZ cubosomal gel indicate a slow release of ATZ from cubosomal dispersion. AUC_{0–48} of oral COL solution was 2.45 ± 1.2 ng.hr/mL, while AUC_{0–48} of ATZ cubosomal gel was 11.85 ± 5.92 ng.hr/mL, and the calculated relative bioavailability of ATZ cubosomal gel, based on AUC_{0–48}, is 4.8367 times compared with ATZ oral solution.

Table 5. Permeation parameters of optimized formulation compared with a solution.

Formula	Jss µg/cm ² .hr	Permeability coefficient (cm/h)	ER ²	ER ³
ATZ Solution	28.64±5.1	0.005±0.002	0.27	1.90
Cubosomal Dispersion	42.37±2.1	0.009±0.001	1.55	1.25
F5	46.51±4.3	0.013±0.002		

Table 6. Bioavailability parameters of optimized formulation compared with a solution.

Formula	ATZ oral Solution	Cubosomal Dispersion	Significance
C_{max} (ng/ml)	0.31±0.17	0.86±0.23	0.031
T_{max} (hr)	3.15±1.82	13.80±4.60	0.042
AUC _{0–48} (ng.hr/mL)	2.45±1.2	11.85±5.92	0.0245

The exact mechanism for the enhanced skin penetration from cubosomal nanoparticles is still under investigation. However, the statistically significant increase ($P < 0.05$) in the relative bioavailability of the transdermal cubosomal dispersions may be due to its structure and its similarity to the skin, which provides high flexibility in transdermal drug delivery for both hydrophilic and lipophilic drugs. Another factor is the penetration enhancer effect of

GMO, which acts by modifying the intercellular ordered structure of lipid bilayer in the stratum corneum and increasing its fluidity.

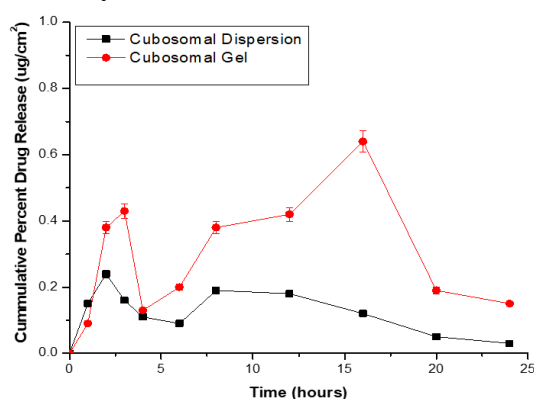


Figure 8. ATZ plasma concentration-time curves in rats after administering a single dose (0.02 mg/kg) of oral ATZ solution and topical ATZ cubosomal gel. Mean (\pm SD, n = 6).

Moreover, the presence of Pluronic F127 in cubosomes allows the drug to penetrate deeply into the stratum corneum, change in the lipid arrangement, improving fluidity, and finally enhancing transdermal drug permeation. Also, the higher skin permeability of cubosomes may be attributed to the bio-adhesive characteristic and permeation enhancement of their building units. The previous results agreed with several literature works that have reported the potential of cubosomes in increasing the transdermal absorption of different drugs such as etodolac, indomethacin, vitamin K, triclosan, and vaccine derived from peptide. Contrary to the earlier reports, cubosomes may improvise the penetration of drugs, and GMO-based cubosomes loaded with capsaicin decreased the skin absorption compared to that of conventional creams.

4. Conclusions

Transdermal cubosomal gel was developed for enhancing the oral bioavailability of ATZ drug. It was apparent that cubosomes containing ATZ are potential in delivering the ATZ through the transdermal route for overcoming the side effects of oral administration. Moreover, cubosomes containing ATZ duplicated the percent of ATZ deposited in the skin, which is favored when deposition of ATZ in the skin is needed. But, because of the large variations in its bioavailability, it is recommended to use many volunteers to obtain more accurate pharmacokinetic parameters.

Funding

This research received no external funding.

Acknowledgments

The authors would like to thank Hetero Drugs. Pvt Ltd. Hyderabad for their enormous support and providing the API as a gift sample. The authors would like to thank Anurag University Chairman and Management for encouraging Research and Development. Vinod Kumar Yata would like to thank the Department of Biotechnology, Government of India, for providing financial support from “DBT-RA Program in Biotechnology & Life Sciences”.

Conflicts of Interest

The authors declare no conflict of interest.

References

1. Danaei, M.; Dehghankhold, M.; Ataei, S.; Davarani, S.F.; Javanmard, R.; Dokhani, A. Impact of particle size and polydispersity index on the clinical applications of lipidic nanocarrier systems. *Pharmaceutics* **2018**, *10*, <https://doi.org/10.3390/pharmaceutics10020057>.
2. Tzeyung, A.S.; Shadab, M.; Bhattamisra, S.K. Fabrication, optimization, and evaluation of rotigotine-loaded chitosan nanoparticles for nose-to-brain delivery. *Pharmaceutics* **2019**, *11*, <https://doi.org/10.3390/pharmaceutics11010026>.
3. Rasti, B.; Jinap, S.; Mozafari, M.R.; Abd-Manap, M.Y. Optimization on preparation condition of polyunsaturated fatty acids nanoliposome prepared by Mozafari method. *J. Liposome Res* **2014**, *24*, 99–105, <https://doi.org/10.3109/08982104.2013.839702>.
4. Gaballa, S.A.; Omar, H.E.G.; Abdelkader, H. Cubosomes: composition, preparation, and drug delivery applications. *J Adv Biomed Pharm Sci* **2020**, *3*, 1–9, <https://doi.org/10.21608/jabps.2019.16887.1057>.
5. Nazaruk, E.; Majkowska, Pilip, A.; Bilewicz, R. Lipidic Cubic Phase Nanoparticles Cubosomes for Efficient Drug Delivery to Cancer Cells. *Chem. Plus. Chem* **2017**, *82*, 570–575, <https://doi.org/10.1002/cplu.201600534>.
6. Nasr, M.; Younes, H.; Abdel-Rashid, R.S. Formulation and evaluation of cubosomes containing colchicine for transdermal delivery. *Drug Deliv and Transl. Res* **2020**, *10*, 1302–1313, <https://doi.org/10.1007/s13346-020-00785-6>.
7. Omar, S.M.; Ismail, A.; Hassanin, K.D.; Dawoud, S.H. Formulation and Evaluation of Cubosomes as Skin Retentive System for Topical Delivery of Clotrimazole. *J. Adv. Pharm. Res* **2019**, *3*, 68–82, <https://doi.org/10.21608/APRH.2019.9839.1079>.
8. Rapalli, V.K.; Banerjee, S.; Khan, S.; Jha, P.N.; Gupta, G.; Dua, K.; Hasnain, M.S.; Nayak, A.K.; Dubey, S.K.; Singhvi, G. QbD-driven formulation development and evaluation of topical hydrogel containing ketoconazole loaded cubosomes. *Materials Science and Engineering: C* **2021**, *119*, <https://doi.org/10.1016/j.msec.2020.111548>.
9. Bhaskar, K.; Sunil, J.; Satveer, J. Formulation and Evaluation of Resveratrol Loaded Cubosomal Nanoformulation for Topical Delivery. *Current Drug Delivery* **2020**, *17*, 1–12, <https://doi.org/10.2174/1567201817666200902150646>.
10. Nasr, M.; Teiama, M.; Ismail, A. In vitro and in vivo evaluation of cubosomal nanoparticles as an ocular delivery system for fluconazole in treatment of keratomycosis. *Drug Deliv and Transl. Res* **2020**, *10*, 1841–1852, <https://doi.org/10.1007/s13346-020-00830-4>.
11. Peng, X.; Zhou, Y.; Han, K.; Qin, L.; Dian, L.; Li, G. Characterization of cubosomes as a targeted and sustained transdermal delivery system for capsaicin. *Drug Des DevelTher* **2015**, *9*, 4209–4218, <https://doi.org/10.2147/DDDT.S86370>.
12. Gupta, S.; Kesarla, R.; Omri, A. Approaches for CNS delivery of drugs–nose to brain targeting of antiretroviral agents as a potential attempt for complete elimination of major reservoir site of HIV to aid AIDS treatment. *Expert Opin Drug Deliv* **2019**, *16*, 287–300, <https://doi.org/10.1080/17425247.2019.1583206>.
13. Eldeeb, A.E.; Salah, S.; Ghorab, M. Formulation and evaluation of cubosomes drug delivery system for treatment of glaucoma: Ex-vivo permeation and in-vivo pharmacodynamic study. *Journal of Drug Delivery Science and Technology* **2019**, *52*, 236–247, <https://doi.org/10.1016/j.jddst.2019.04.036>.
14. Gaballa, S.A.; Garhy, O.H.E.; Moharram, H. Preparation and Evaluation of Cubosomes/Cubosomal Gels for Ocular Delivery of BeclomethasoneDipropionate for Management of Uveitis. *Pharm Res* **2020**, *37*, <https://doi.org/10.1007/s11095-020-02857-1>.
15. Sharma, A.; Kumar, L.; Kumar, P.; Prasad, N.; Rastogi, V. Niosomes: A Promising Approach in Drug Delivery Systems. *J Drug Del Therap* **2019**, *9*, 635–42, <https://doi.org/10.22270/jddt.v9i4.3064>.
16. Armia, S.; Garhy, O.; Abdelkader, H. Cubosomes: composition, preparation, and drug delivery applications. *Journal of advanced Biomedical and Pharmaceutical Sciences* **2019**, *3*, 1–9, <https://doi.org/10.21608/jabps.2019.16887.1057>.
17. von Halling Laier, C.; Gibson, B.; van de Weert, M.; Boyd, B.J.; Rades, T.; Boisen, A.; Hook, S.; Nielsen, L.H. Spray dried cubosomes with ovalbumin and Quil-A as a nanoparticulate dry powder vaccine formulation. *International Journal of Pharmaceutics* **2018**, *550*, 35–44, <https://doi.org/10.1016/j.ijpharm.2018.08.036>.
18. Salah, S.; Mahmoud, A.A.; Kamel, A.O. Etodolac transdermal cubosomes for the treatment of rheumatoid arthritis: ex vivo permeation and in vivo pharmacokinetic studies. *Drug Delivery* **2017**, *24*, 846–856, <https://doi.org/10.1080/10717544.2017.1326539>.

19. Gaballa, S.A.; El Garhy, O.H.; Moharram, H.; Abdelkader, H. Preparation and Evaluation of Cubosomes/Cubosomal Gels for Ocular Delivery of Beclomethasone Dipropionate for Management of Uveitis. *Pharmaceutical Research* **2020**, *37*, <https://doi.org/10.1007/s11095-020-02857-1>.
20. Yasser, M.; Teaima, M.; El-Nabarawi, M.; El-Monem, R.A. Cubosomal based oral tablet for controlled drug delivery of telmisartan: formulation, in-vitro evaluation and in-vivo comparative pharmacokinetic study in rabbits. *Drug Development and Industrial Pharmacy* **2019**, *45*, 981-994, <https://doi.org/10.1080/03639045.2019.1590392>.
21. Sana, K.; Poorva, J.; Sourabh, J.; Richa, J.; Saurabh, B.; Aakanchha, J. Topical Delivery of Erythromycin Through Cubosomes for Acne. *Pharmaceutical Nanotechnology* **2018**, *6*, 38-47, <https://doi.org/10.2174/2211738506666180209100222>.
22. Håkansson, J.; Ringstad, L.; Umerska, A.; Johansson, J.; Andersson, T.; Boge, L.; Rozenbaum, R.T.; Sharma, P.K.; Tollbäck, P.; Björn, C.; Saulnier, P.; Mahlapuu, M. Characterization of the in vitro, ex vivo, and in vivo Efficacy of the Antimicrobial Peptide DPK-060 Used for Topical Treatment. *Front Cell Infect. Microbiol* **2019**, *9*, <https://doi.org/10.3389/fcimb.2019.00174>.
23. Kundu, S.; Kumari, N.; Soni, S.R.; Ranjan, S.; Kumar, R.; Sharon, A.; Ghosh, A. Enhanced Solubility of Telmisartan Phthalic Acid Cocrystals within the pH Range of a Systemic Absorption Site. *ACS Omega* **2018**, *3*, 15380-15388, <https://doi.org/10.1021/acsomega.8b02144>.
24. Mannava, M.K.C.; Suresh, K.; Nangia, A. Enhanced Bioavailability in the Oxalate Salt of the Anti-Tuberculosis Drug Ethionamide. *Crystal Growth & Design* **2016**, *16*, 1591-1598, <https://doi.org/10.1021/acs.cgd.5b01700>.
25. Ferramosca, A.; Treppiccione, L.; Di Giacomo, M.; Aufiero, V.R.; Mazzarella, G.; Maurano, F.; Gerardi, C.; Rossi, M.; Zara, V.; Mita, G.; Bergamo, P. Prunus Mahaleb Fruit Extract Prevents Chemically Induced Colitis and Enhances Mitochondrial Oxidative Metabolism via the Activation of the Nrf2 Pathway. *Molecular Nutrition & Food Research* **2019**, *63*, <https://doi.org/10.1002/mnfr.201900350>.
26. Salah, S.; Mahmoud, A.A.; Kamel, A.O. Etodolac transdermal cubosomes for the treatment of rheumatoid arthritis: ex vivo permeation and in vivo pharmacokinetic studies. *Drug Delivery* **2017**, *24*, 846-856, <https://doi.org/10.1080/10717544.2017.1326539>.
27. Nasr, M.; Younes, H.; Abdel-Rashid, R.S. Formulation and evaluation of cubosomes containing colchicine for transdermal delivery. *Drug Delivery and Translational Research* **2020**, *10*, 1302-1313, <https://doi.org/10.1007/s13346-020-00785-6>.
28. Kovvasu, S.P.; Kunamaneni, P.; Yeung, S.; Kodali, B. Determination of colchicine in human plasma by a sensitive LC-MS/MS assay. *World J Pharm Sci* **2018**, *7*, 35-44.
29. Danaei, M.; Dehghankhold, M.; Ataie, S.; Hasanzadeh Davarani, F.; Javanmard, R.; Dokhani, A.; Khorasani, S.; Mozafari, M.R. Impact of Particle Size and Polydispersity Index on the Clinical Applications of Lipidic Nanocarrier Systems. *Pharmaceutics* **2018**, *10*, <https://doi.org/10.3390/pharmaceutics10020057>.
30. Dai, Q.; Yang, Y.; Chen, K.; Cheng, Z.; Ni, Y.; Li, J. Optimization of Supercritical CO₂ Operative Parameters to Simultaneously Increase the Extraction Yield of Oil and Pentacyclic Triterpenes from Artichoke Leaves and Stalks by Response Surface Methodology and Ridge Analysis. *European Journal of Lipid Science and Technology* **2019**, *121*, <https://doi.org/10.1002/ejlt.201800120>.
31. Meng, Q.; Wang, A.; Hua, H.; Jiang, Y.; Wang, Y.; Mu, H.; Wu, Z.; Sun, K. Intranasal delivery of Huperzine A to the brain using lactoferrin-conjugated N-trimethylated chitosan surface-modified PLGA nanoparticles for treatment of Alzheimer's disease. *Int J Nanomedicine* **2018**, *13*, 705-718, <https://doi.org/10.2147/IJN.S151474>.
32. Gaballa, S.A.; El Garhy, O.H.; Moharram, H.; Abdelkader, H. Preparation and Evaluation of Cubosomes/Cubosomal Gels for Ocular Delivery of Beclomethasone Dipropionate for Management of Uveitis. *Pharmaceutical Research* **2020**, *37*, <https://doi.org/10.1007/s11095-020-02857-1>.
33. Shi, X.; Peng, T.; Huang, Y.; Mei, L.; Gu, Y.; Huang, J.; Han, K.; Li, G.; Hu, C.; Pan, X.; Wu, C. Comparative studies on glycerol monooleate- and phytantriol-based cubosomes containing oridonin in vitro and in vivo. *Pharmaceutical Development and Technology* **2017**, *22*, 322-329, <https://doi.org/10.3109/10837450.2015.1121496>.
34. Patil, R.P.; Pawara, D.D.; Gudewar, C.S.; Tekade, A.R. Nanostructured cubosomes in an in situ nasal gel system: an alternative approach for the controlled delivery of donepezil HCl to brain. *Journal of Liposome Research* **2019**, *29*, 264-273, <https://doi.org/10.1080/08982104.2018.1552703>.
35. Muntimadugu, E.; Dhommatti, R.; Jain, A.; Challa, V.G.S.; Shaheen, M.; Khan, W. Intranasal delivery of nanoparticle encapsulated tarenflurbil: A potential brain targeting strategy for Alzheimer's disease. *European Journal of Pharmaceutical Sciences* **2016**, *92*, 224-234, <https://doi.org/10.1016/j.ejps.2016.05.012>.